13th ewtec 2019 Proceedings of the 13th European Wave and Tidal Energy Conference 1-6 Sept 2019, Naples, Italy

Geometric optimization of a hinge-barge wave energy converter

LiGuo Wang, and John V. Ringwood

***Abstract*—Based on a small prototype of the McCabe wave pump device, this paper studies the optimal size of an interconnected pontoon system, where the power take-off systems attached to each barge are equipped with optimal linear passive dampers. To this end, an optimization procedure is developed, where the objective is to maximize the extracted energy of the device under given sea states. A multi-DOF mathematical model is presented to describe the device motion, and associated hydrodynamic parameters are computed using a boundary element model tool, based on linear potential flow theory. Numerical results, under regular and irregular waves, are presented. Simulation results show that the optimal dimension of the device, under given sea states, can be found using the developed methodology. In addition, it is found that the three-body hinge-barge device tends to perform like a two-body system under optimal control conditions. This indicates that a two-barge control system may be a better design solution in those situations, considering the high cost of power take-off systems.**

***Index Terms*—Multi-body wave energy converters, hinge barge, geometry optimization, energy maximizing control, optimal linear passive control.**

I. Introduction

A Number of studies have been done on the geometric optimization of wave energy converters (WECs), aiming to improve their energy extraction from incident waves. In [1], the authors optimize the geometric shape and the radius of a floating WEC, using an average annual wave energy spectrum of its design location at the Atlantic marine energy test site as the input. In [2], the optimal diameter and draft of a one-body heaving point absorber are investigated for the nearshore region of Rio De Janeiro, and the optimization process is based on a frequency-domain model and aims at maximizing both absorbed energy and absorption bandwidth when providing a natural period close to the predominant wave periods of the sea site. In [3], the authors perform geometric optimization for a conical-bottom buoy with three types of PTO which are linear, constant, and quadratic non-linear, using the commercial software Flow-3D. A genetic algorithm is also applied in the geometric optimization of WECs [4] [5] [6].

However, most of these geometric optimization studies are performed independently of the control system, and little convergence has been reached in design principle. Recently, a more holistic approach is proposed for WEC geometry design and optimization, i.e. the control strategy employed by the power take-off system (PTO) is informed in the design stage of the device geometry. In [7] [8] [9], control-informed geometric design (CIGD) is investigated for a single WEC that employs a 1-DOF cylinder as the absorber, considering its radius and draft as the design parameters to be optimized, and results indicate that optimal geometry can be obtained depending on the type of PTO control strategies employed at the design optimization stage of the device. In [10], control-informed geometric optimization is performed for a wave farm consisting of multiple identical 1-DOF WECs, and results show that a layout optimized without knowledge of the control system to be used can be inferior to the extent of recovering 40% less energy than the considered farm layout optimized with knowledge of the control system.

This paper focuses on geometric optimization of a multi-body hinge-barge WEC, using the CIGD approach. Hinge-barge WECs are composed of an assembly of joints, and designed to operate along the propagation direction of incident waves. To date, a number of hinge-barge WECs has been proposed, e.g., the SeaPower WEC, the Mocean WEC, the M4 WEC [11] and the McCabe Wave Pump device [12]. Their performance is studied through numerical simulations and verified by physical experiments. Results indicate that this type of WEC usually has a broad frequency response range and a high capture width ratio [13] [14]. However, limited work has been done to optimize the geometric size and it is still not clear whether two pontoons or three pontoons are the best, or what the optimal dimensions are, in particular considering the control strategies employed by the power take-off (PTO) system. In this paper, the candidate device used in study is originally from the McCabe Wave Pump WEC [15].

The remainder of the paper is organized as follows: in Section II, the method used for geometric optimization of the hinge-barge WEC is briefly presented. In Section III, the mathematical model, based on Lagrangian mechanics, is explained. Section IV explains the optimization methodology of PTO control parameters. Section V illustrates the detailed geometric optimization procedure. In Section VI, the proposed optimization procedure is applied to a small-scale prototype and corresponding numerical simulation results are presented. Finally, discussions are presented in Section VII and conclusions are drawn in Section VIII.

Paper ID number: 1389- Conference track: WHM

L. Wang is with the Centre for Ocean Energy Research, National University of Ireland Maynooth, Maynooth, Ireland, and also with the Marine and Renewable Energy Ireland. (e-mail: Liguo.Wang@mu.ie).

J. V. Ringwood is with the Centre for Ocean Energy Research, National University of Ireland Maynooth, Maynooth, Ireland (e-mail: John.Ringwood@mu.ie).

II. Method

The proposed geometric optimization aims to find the optimal size of the WEC while incorporating the PTO control strategy at the geometry design stage, which will yield a better performance of the device at the operation stage, in terms of energy production. As the hinge-barge WEC is designed to operate along the propagating direction of incident waves, only the geometric sizes of fore barge and aft barge in the wave propagation direction are considered as geometric optimization variables.

The original three-barge WEC is equipped with two PTO systems, one located between the fore barge and the central barge and the other located between the aft barge and the central barge. It is well known that the control strategy employed by a PTO controller affects the energy production and it further may influence the results of geometric optimization, as indicated in [9]. However, the sensitivity of the optimal geometry to the control strategy is not the focus of the paper. We assume that each PTO system employs a linear passive controller and the associated PTO damping coefficients are optimized for each set of WEC geometry parameters and sea states during the optimization procedure.

Additionally, geometric optimization requires estimating the energy production (as an objective function) of a device under given sea states. To approach that, a multi-DOF mathematical model is required to describe the device dynamics. To model the collection of multiple bodies linked by hinges or by rigid connection, the methodology treats three barges as free-response units in the hydrodynamic model and considers the central barge and the damping plate as one body as they are rigidly connected, then incorporates all the constraints representing the hinge connections in a formulation of motion equations. The hydrodynamic problem is solved based on linear potential flow theory. It has previously been shown the hydrodynamics of hinge barges are predominantly linear [16]. The mathematical model evaluates the wave induced response of the central barge in surge, heave and pitch modes, also allows the computation of the rotation of fore and aft barges relative to the central barge.

The developed mathematical/computational model allows the lengths of fore barge and of aft barge and control forces of fore PTO and of aft PTO to be adjusted. Based on this mathematical model, the PTO forces or the corresponding damping coefficients are optimized during the optimization procedure and the power production is calculated in given sea states, fully considering the hydrodynamic interactions and hinge coupling in all motion modes.

Finally, the optimized geometric sizes, i.e. the fore barge length and the aft barge length, are selected while incorporating the optimal linear passive control strategy at the geometry design optimization stage.

III. Mathematical Modeling

Several mathematical models have been proposed for hinge-barge devices. In [17], the wave-induced response of a two-body hinged system is investigated using a frequency-domain mathematical model, with the constraints in the hinge connection being imposed by the Lagrange multiplier technique. Later on, this method is applied to study the performance of a two-body hinged WEC under regular waves [18]. This augmented formulation using the Lagrange multiplier technique is based on Hamiltonian theory and the dynamic equations are formulated in terms of a set of redundant coordinates. However, the developed frequency-domain based model is not suitable for case studies of irregular waves and for model-based control. In [19], a time-domain model is proposed for a 4-DOF McCabe Wave Pump WEC that moves in heave and pitch, using another popular approach for describing dynamics of multibody systems, i.e. the embedded technique.

In this section, a 5-DOF time-domain model is presented to describe the device's motion in heave, surge and pitch, as well as the relative pith motions of the fore barge and the aft barge to the central barge, using the embedded technique based on Lagrangian mechanics. In addition, the presence of ballast in three barges that influences the center of mass are considered in the hydrodynamic modeling and numerical simulations.

A. Frame of Reference

Figure 1 shows the device used in this study. Three kinds of reference frames are used to describe the dynamics of this multibody system, including one global inertia frame and three local body frames.

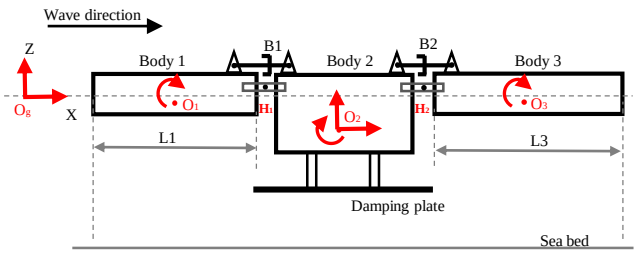

Fig. 1. The three-body hinge-barge WEC used in study [19].

1) Global inertia frame: The global inertia frame is fixed in space and its location and orientation do not change over time. The general displacement of a body in a multibody system is defined by a rotation plus a translation.

2) Local body frame: Each local body frame is fixed to a point of each barge and the point is defined by the user. It is a non-inertial frame of reference and its location and orientation in space vary over time relative to the global inertia frame. For a rigid body, its particles do not move with respect to its local body frame. The configuration of a rigid body in a multibody system is identified by defining the location of the origin and the orientation of the corresponding local body frame with respect to the global inertial frame.

3) Generalized frame: The generalized frame is used when the embedding technique is used to formulate the dynamic equations of constrained multibody systems [20]. A multibody system, consisting of n interconnected rigid bodies, requires $6n$ generalized coordinates in order to describe the system configuration in 3D space. These generalized coordinates are not independent if the hinge constraints exist, and the number of independent generalized coordinates is defined by the number of degrees of freedom of a system.

Independent generalized coordinates are important to understand and control of the motion of a multibody system. Deriving the kinetic energy, force and virtual work expressions in terms of generalized coordinates, the equation of motion eventually is associated with the system-independent coordinates, with constraint forces automatically eliminated using the embedding technique.

The generalized coordinates of the studied three-body hinge-barge WEC, in two-dimensional space, is defined as:

$$\begin{aligned}\boldsymbol{q(t)} &= [q_1, q_2, q_3, q_4, q_5, q_6, q_7, q_8, q_9]^T \\ &= [x_{b1}, z_{b1}, \theta_{b1}, x_{b2}, z_{b2}, \theta_{b2}, x_{b3}, z_{b3}, \theta_{b3}]^T,\end{aligned} \tag{1}$$

where $\boldsymbol{R}^i = [x_{bi}, z_{bi}]^T$ is the global position vector of the origin of the body frame i, and x_{bi} and z_{bi} represent the Cartesian coordinates in the x and z directions, respectively. θ_{bi} is the orientation angle of local body frame i with respect to the global inertia frame.

The multi-body system has 5 DOFs in 2D space, and the independent generalized coordinates are defined as:

$$\boldsymbol{q}_s(t) = [\theta_{b1}(t), x_{b2}(t), z_{b2}(t), \theta_{b2}(t), \theta_{b3}(t)]^T. \tag{2}$$

B. Center of Mass and Inertia Matrix

It is well known that the mass of each barge influences its hydrodynamic characteristics and system dynamics, and center of mass also influences the evaluation of generalized forces associated with independent generalized coordinates. For the studied prototype, ballast is used in each barge to lower its center of mass and to increase stability. The center of mass of each barge is therefore not located at the centroid.

The inertia matrix of body i is defined as:

$$\boldsymbol{M}^i = \begin{bmatrix} m^i & 0 & m^i z_g^i \\ 0 & m^i & -m^i x_g^i \\ m^i z_g^i & -m^i x_g^i & I_{yy}^i \end{bmatrix}, \tag{3}$$

where m^i is the inertia mass of body i, and $(x_g^i, z_g^i)^T$ is the position vector of the center of mass of body i defined in the local body frame i. I_{yy}^i is the moment of inertia of body i defined in local body frame i.

As indicated in Eq. (3), the mass matrix of a rigid body will become diagonal if the origin of the body frame is fixed to the center of mass of the body, which also results in the elimination of off-diagonal terms during the transformation from the Cartesian frame to the generalized frame. Therefore, for simplicity, and for eliminating the inertial coupling between the rotation and translation of each body frame, the origin of each local body frame is attached to the center of mass of each barge. Table I lists the distance of the vertical center of each barge mass with respect to its bottom surface.

TABLE I
VERTICAL DISTANCE OF CENTER OF MASS OF EACH BARGE TO ITS BOTTOM SURFACE

Property	Value
Fore barge	4 cm
Central barge	5 cm
Aft barge	4 cm

C. Hinge Constraints

For a hinge joint H_k between a planar body i and a planar body j in a multibody system, the hinge constraint allows only relative pitch motion between the two bodies. The hinge constraint is defined as: the global position of the hinge point H_k, defined by the set of coordinates of body i, equals the global position of point H_k defined by the set of coordinates of body j, i.e. $\boldsymbol{r}^i = \boldsymbol{r}^j$.

The global position vector of the hinge point, defined through body frame i, is expressed in terms of a translation and a rotation, and given by

$$\boldsymbol{r}^i = \boldsymbol{R}^i + \boldsymbol{A}^i \bar{\boldsymbol{H}}_k^i, \tag{4}$$

where $\bar{\boldsymbol{H}}_k^i = (h_x^{ik}, h_z^{ik})^T$ is a local position vector of hinge point H_k, defined in body frame $\boldsymbol{o}^i$, is constant in the case of rigid body analysis, and $\boldsymbol{R}^i$ is the global position vector of the origin $\boldsymbol{o}^i$ of the body frame i. $\boldsymbol{A}^i$ is the transformation matrix from local body frame i to the global inertial frame.

The global position vector of the hinge point, defined through body frame j, is:

$$\boldsymbol{r}^j = \boldsymbol{R}^j + \boldsymbol{A}^j \bar{\boldsymbol{H}}_k^j, \tag{5}$$

where $\bar{\boldsymbol{H}}_k^j$ is a local position vector of hinge point H_k defined in body frame j. The transformation matrix from local body frame j to the global frame is:

$$\boldsymbol{A}^j = \begin{bmatrix} cos(\theta_j) & -sin(\theta_j) \\ sin(\theta_j) & cos(\theta_j) \end{bmatrix}. \tag{6}$$

For small amplitude of pitch rotation, the transformation matrix can be linearized using $cos(\theta_j) \approx 1$ and $sin(\theta_j) \approx \theta_j$.

D. Equation of Motion

Based on the D'Alembert-Lagrange equation, the equation of motion of the hinge-barge WEC is expressed [19] as:

$$\begin{aligned}&\boldsymbol{M}_s \dot{\boldsymbol{V}}_s(t) + (\boldsymbol{B}_s + \boldsymbol{B}_{visc,s})\boldsymbol{V}_s(t) + \boldsymbol{G}_s \boldsymbol{X}_s(t) + \boldsymbol{M}_{\infty s} \dot{\boldsymbol{V}}_s(t) \\ &+ \int_0^t \boldsymbol{K}_s(t-\tau)\boldsymbol{V}_s(\tau)d\tau = \boldsymbol{F}_{es}(t) + \boldsymbol{F}_{us}(t),\end{aligned} \tag{7}$$

$$
\begin{aligned}
&\boldsymbol{M}_s = \boldsymbol{P}^T \boldsymbol{M} \boldsymbol{P},\\
&\boldsymbol{B}_s = \boldsymbol{P}^T \boldsymbol{B} \boldsymbol{P} + \boldsymbol{P}^T \boldsymbol{M} \dot{\boldsymbol{P}} + \boldsymbol{P}^T \boldsymbol{M}_\infty \dot{\boldsymbol{P}},\\
&\boldsymbol{B}_{visc,s} = \boldsymbol{P}^T \boldsymbol{B}_{visc} \boldsymbol{P},\\
&\boldsymbol{G}_s = \boldsymbol{P}^T \boldsymbol{G} \boldsymbol{P},\\
&\boldsymbol{M}_{\infty s} = \boldsymbol{P}^T \boldsymbol{M}_\infty \boldsymbol{P},\\
&\boldsymbol{K}_s = \boldsymbol{P}^T \boldsymbol{K} \boldsymbol{P},\\
&\boldsymbol{F}_{es} = \boldsymbol{P}^T \boldsymbol{F}_e,\\
&\boldsymbol{F}_{us} = \boldsymbol{P}^T \boldsymbol{F}_u,
\end{aligned}
\tag{8}
$$

where $\boldsymbol{M} = diag(\boldsymbol{M}^1, \boldsymbol{M}^2, \boldsymbol{M}^3)$ is the mass matrix and $\boldsymbol{M}_s$ is the generalized mass matrix associated with independent generalized coordinates, $\boldsymbol{M}_\infty$ is the matrix of added mass at infinite frequency, $\boldsymbol{P}$ is the system Jacobian matrix, $\boldsymbol{B}_{visc} = diag(\boldsymbol{B}^1_{visc}, \boldsymbol{B}^2_{visc}, \boldsymbol{B}^3_{visc})$ is the linearized viscous damping matrix, $\boldsymbol{B}_s = diag(\boldsymbol{B}^1_s, \boldsymbol{B}^2_s, \boldsymbol{B}^3_s)$ is the Coriolis-Centripetal matrix, $\boldsymbol{G} = diag(\boldsymbol{G}^1, \boldsymbol{G}^2, \boldsymbol{G}^3)$ is the total hydrostatic matrix, $\boldsymbol{F}_e(t) = [(\boldsymbol{F}^1_e)^T, (\boldsymbol{F}^2_e)^T, (\boldsymbol{F}^3_e)^T]^T$ is the matrix of generalized excitation force with $\boldsymbol{F}^i_e = (F^i_{ex}, F^i_{ez})^T$ representing the wave excitation force vector related to the generalized coordinates of body i.

The PTO force vector is:

$$
\boldsymbol{F}_u(t) = \boldsymbol{F}_P \boldsymbol{U}_c(t) = \boldsymbol{F}_P [u_1(t), u_2(t)]^T, \tag{9}
$$

where $u_1(t)$ and $u_2(t)$ represent the PTO control force applied at fore PTO and aft PTO, respectively.

The PTO control configuration matrix $\boldsymbol{F}_P$ [21] is defined as:

$$
\boldsymbol{F}_P^T = \begin{bmatrix} 0 & 1 & 0 & -1 & 0 & 0 \\ 0 & 0 & 0 & -1 & 0 & 1 \end{bmatrix}. \tag{10}
$$

The independent velocity vector, $\boldsymbol{V}_s(t)$, is defined through:

$$
\boldsymbol{V}(t) = \boldsymbol{P} \boldsymbol{V}_s(t). \tag{11}
$$

Matrix $\boldsymbol{P}$ is derived from the linearized kinematic constraint equations and expressed as:

$$
\boldsymbol{P} = \begin{bmatrix}
h^{11}_z & 1 & 0 & -h^{21}_z & 0 \\
-h^{11}_x & 0 & 1 & h^{21}_x & 0 \\
1 & 0 & 0 & 0 & 0 \\
0 & 1 & 0 & 0 & 0 \\
0 & 0 & 1 & 0 & 0 \\
0 & 0 & 0 & 1 & 0 \\
0 & 1 & 0 & -h^{22}_z & h^{32}_z \\
0 & 0 & 1 & h^{22}_x & -h^{32}_x \\
0 & 0 & 0 & 0 & 1
\end{bmatrix}. \tag{12}
$$

If the pitch velocities of the fore and of aft barges in $\boldsymbol{V}_s(t)$ are defined relative to the pitch of the central barge, the system Jacobian matrix is defined as:

$$
\boldsymbol{P} = \begin{bmatrix}
h^{11}_z & 1 & 0 & -h^{21}_z + h^{11}_z & 0 \\
-h^{11}_x & 0 & 1 & h^{21}_x - h^{11}_x & 0 \\
1 & 0 & 0 & 1 & 0 \\
0 & 1 & 0 & 0 & 0 \\
0 & 0 & 1 & 0 & 0 \\
0 & 0 & 0 & 1 & 0 \\
0 & 1 & 0 & -h^{22}_z + h^{32}_z & h^{32}_z \\
0 & 0 & 1 & h^{22}_x - h^{32}_x & -h^{32}_x \\
0 & 0 & 0 & 1 & 1
\end{bmatrix}. \tag{13}
$$

The linearized viscous matrix is identified from experimental and simulation results. More details are given in [22].

$$
\min_{\boldsymbol{B}_{visc,s}} \quad J_{LS} = \sum_{i=1}^{n_f} \sum_{j=1}^{n} |H_j(w_i) - \hat{H}_j(w_i)|^2, \tag{14}
$$

where n_f is the number of frequencies of the spectrum of the incident waves, n is the number of degrees of freedom, H_j and $\hat{H}_j$ are the experimental, and theoretical, transfer functions between the j^{th} DOF and the incident wave, respectively.

IV. Control parameter optimization

Both spectral and pseudo-spectral methods can be used to compute an approximate solution of the equation of motion. [23] presents the pseudo-spectral approach while this section illustrates the spectral method for approximating the solution.

States and control variables are represented by a linear combination of basis functions. Here, truncated zero-mean Fourier series are used to approximate the velocity and PTO control forces, and the basis functions are defined as:

$$
\boldsymbol{\Phi} = [cos(w_0 t)\ sin(w_0 t)\ ...\ cos(n w_0 t)\ sin(n w_0 t)]^T, \tag{15}
$$

where w_0 is the fundamental angular frequency.

The i^{th} components of the position and velocity vectors, are given, respectively, as follows:

$$
x_i(t) \approx \boldsymbol{\Phi}^T(t) \hat{\boldsymbol{x}}_i, \tag{16}
$$

$$
v_i(t) \approx \boldsymbol{\Phi}^T(t) \hat{\boldsymbol{v}}_i, \tag{17}
$$

where $\hat{\boldsymbol{x}}_i = [\hat{x}_1,\ \hat{x}_2,\ ...,\ \hat{x}_{N_{dc}}]^T$ and $\hat{\boldsymbol{v}}_i = [\hat{v}_1,\ \hat{v}_2,\ ...\ \hat{v}_{N_{dc}}]^T$ are the Fourier projection vectors of displacement and velocity of mode i, respectively.

The total displacement and velocity vectors are formulated, respectively, as follows:

$$
\begin{aligned}
\boldsymbol{X}_s(t) &= [x_1(t),\ x_2(t),\ ...,\ x_{Ndc}(t)]^T \\
&\approx [\boldsymbol{\Phi}^T \hat{\boldsymbol{x}}_1,\ \boldsymbol{\Phi}^T \hat{\boldsymbol{x}}_2,\ ...,\ \boldsymbol{\Phi}^T \hat{\boldsymbol{x}}_{N_{dc}}]^T \\
&= \boldsymbol{\Psi}(t) \hat{\boldsymbol{X}}_s,
\end{aligned}
\tag{18}
$$

$$
\begin{aligned}
\boldsymbol{V}_s(t) &= [v_1(t),\ v_2(t),\ ...,\ v_{Ndc}(t)]^T \\
&\approx [\boldsymbol{\Phi}^T \hat{\boldsymbol{v}}_1,\ \boldsymbol{\Phi}^T \hat{\boldsymbol{v}}_2,\ ...,\ \boldsymbol{\Phi}^T \hat{\boldsymbol{v}}_{N_{dc}}]^T \\
&= \boldsymbol{\Psi}(t) \hat{\boldsymbol{V}}_s,
\end{aligned}
\tag{19}
$$

where $\boldsymbol{\Psi}(t) = \boldsymbol{I}_{N_{dc}} \otimes \boldsymbol{\Phi}^T$ is a N_{dc} block diagonal matrix and its each block is $\boldsymbol{\Phi}^T$. The symbol $\otimes$ denotes the Kronecker product of two matrices and the symbol $\boldsymbol{I}_{N_{dc}}$ denotes an identity matrix of size N_{dc}. The matrix $\hat{\boldsymbol{X}}_s = [\hat{\boldsymbol{x}}^T_1,\ \hat{\boldsymbol{x}}^T_2,\ ...,\ \hat{\boldsymbol{x}}^T_{N_{bs}}]^T$ and $\hat{\boldsymbol{V}}_s = [\hat{\boldsymbol{v}}^T_1,\ \hat{\boldsymbol{v}}^T_2,\ ...\ , \hat{\boldsymbol{v}}^T_{N_{bs}}]^T$.

The derivatives of displacement and velocity with respect to time are given, respectively, as:

$$
\begin{aligned}
\dot{\boldsymbol{X}}_s(t) &\approx [\dot{\boldsymbol{\Phi}}^T(t) \hat{\boldsymbol{x}}_1,\ \dot{\boldsymbol{\Phi}}^T(t) \hat{\boldsymbol{x}}_2,\ ...,\ \dot{\boldsymbol{\Phi}}^T(t) \hat{\boldsymbol{x}}_{N_{dc}}(t)]^T \\
&= [\boldsymbol{\Phi}^T(t) \boldsymbol{D} \hat{\boldsymbol{x}}_1,\ \boldsymbol{\Phi}^T(t) \boldsymbol{D} \hat{\boldsymbol{x}}_2,\ ...,\ \boldsymbol{\Phi}^T(t) \boldsymbol{D} \hat{\boldsymbol{x}}_{N_{dc}}]^T \\
&= \boldsymbol{\Psi}(t) \boldsymbol{D}_{dc} \hat{\boldsymbol{X}}_s,
\end{aligned}
\tag{20}
$$

$$\dot{\boldsymbol{V}}_s(t) = \boldsymbol{\Psi}(t)\boldsymbol{D}_{dc}\hat{\boldsymbol{V}}_s, \tag{21}$$

where $\boldsymbol{D}_{dc} = \boldsymbol{I} \otimes \boldsymbol{D}$. The differential matrix $\boldsymbol{D} \in R^{N_{bs}\times N_{bs}}$ is block diagonal, and each diagonal block $\boldsymbol{D}^k$ with $k = 1, 2, ..., N_{bs}/2$ is

$$\boldsymbol{D}^k = \begin{bmatrix} 0 & kw_0 \\ -kw_0 & 0 \end{bmatrix}. \tag{22}$$

The PTO control force is expressed as:

$$\begin{aligned} \boldsymbol{F}_{us}(t) &= \boldsymbol{P}^T\boldsymbol{F}_P[\boldsymbol{\Phi}^T(t)\hat{\boldsymbol{u}}_1, \boldsymbol{\Phi}^T(t)\hat{\boldsymbol{u}}_2]^T \\ &= \boldsymbol{P}^T\boldsymbol{F}_P\boldsymbol{\Psi}_{2*2N_{bs}}\hat{\boldsymbol{U}}_c, \end{aligned} \tag{23}$$

where $\boldsymbol{\Psi}_{2*2N_{bs}} = \boldsymbol{I}_2 \otimes \boldsymbol{\Phi}^T$ and $\hat{\boldsymbol{U}}_c = [\hat{\boldsymbol{u}}_1^T, \hat{\boldsymbol{u}}_2^T]^T$. $\hat{\boldsymbol{u}}_i = [\hat{u}_1,\ \hat{u}_2,\ ...,\ \hat{u}_{N_{bs}}]^T$ is the control Fourier projection vector.

Substituting Eqs. (18), (19), (21) and (23) into Eq. (7), the equation of motion is re-formulated in a residual form:

$$\begin{aligned} &\boldsymbol{r}(t) = (\boldsymbol{M}_s + \boldsymbol{M}_{\infty s})\boldsymbol{\Psi}(t)\boldsymbol{D}_{dc}\hat{\boldsymbol{V}}_s + (\boldsymbol{B}_s + \boldsymbol{B}_{visc,s})\boldsymbol{\Psi}(t)\hat{\boldsymbol{V}}_s \\ &+ \boldsymbol{G}_s\boldsymbol{\Psi}(t)\hat{\boldsymbol{X}}_s + \int_0^t \boldsymbol{K}(t-\tau)\boldsymbol{\Psi}(\tau)\hat{\boldsymbol{V}}_s d\tau - \boldsymbol{P}^T\boldsymbol{\Psi}_e(t)\hat{\boldsymbol{E}} - \\ &\boldsymbol{P}^T\boldsymbol{F}_P\boldsymbol{\Psi}_{2*2N_{bs}}\hat{\boldsymbol{U}}_c, \end{aligned} \tag{24}$$

where $\boldsymbol{r}$ is a vector of size $N_{dc}\times 1$, and its i^{th} component is:

$$\begin{aligned} &r_i(t) = \sum_{p=1}^{N_{dc}}[(\boldsymbol{M}_s + \boldsymbol{M}_{\infty s})_{i,p}\boldsymbol{\Phi}^T(t)\boldsymbol{D}\hat{\boldsymbol{v}}_p + (\boldsymbol{G}_s)_{i,p}\boldsymbol{\Phi}^T(t)\hat{\boldsymbol{x}}_p \\ &+ (\boldsymbol{B}_s + \boldsymbol{B}_{visc,s})_{i,p}\boldsymbol{\Phi}^T(t)\hat{\boldsymbol{v}}_p + \int_0^t K_{i,p}(t-\tau)\boldsymbol{\Phi}^T(\tau)\hat{\boldsymbol{v}}_p d\tau] \\ &- (\boldsymbol{P}^T\boldsymbol{\Psi}_e(t)\hat{\boldsymbol{E}})_i - (\boldsymbol{P}^T\boldsymbol{F}_P\boldsymbol{\Psi}_{2*2N_{bs}}\hat{\boldsymbol{U}}_c)_i. \end{aligned} \tag{25}$$

The residual form of the equation of motion is minimized by solving

$$\begin{aligned} &\langle \phi_j, r_i \rangle = 0, \\ &\langle \boldsymbol{\Phi}, r_i \rangle = \boldsymbol{0}_{N_{bs}\times 1}. \end{aligned} \tag{26}$$

The discretized equation of motion becomes a linear system:

$$\boldsymbol{H}\hat{\boldsymbol{V}}_s = \boldsymbol{L}\hat{\boldsymbol{E}}_s + \boldsymbol{C}\hat{\boldsymbol{U}}_c, \tag{27}$$

with $\boldsymbol{H}$ is a block matrix with $N_{dc} \times N_{dc}$ blocks:

$$\boldsymbol{H} = \begin{bmatrix} \boldsymbol{H}_{1,2} & ... & \boldsymbol{H}_{1,N_{dc}} \\ \vdots & & \vdots \\ \boldsymbol{H}_{N_{dc},1} & ... & \boldsymbol{H}_{N_{dc},N_{dc}} \end{bmatrix}, \tag{28}$$

and

$$\begin{aligned} &\boldsymbol{H}_{i,p} = (\boldsymbol{M}_s + \boldsymbol{M}_{\infty s})_{i,p}\boldsymbol{D} + (\boldsymbol{B}_s + \boldsymbol{B}_{visc,s})_{i,p}\boldsymbol{I}_{N_{bs}} \\ &+ (\boldsymbol{G}_s)_{i,p}\boldsymbol{D}^{-1} + \boldsymbol{G}_{i,p}. \end{aligned} \tag{29}$$

$\boldsymbol{L}$ is a block matrix:

$$\boldsymbol{L} = \begin{bmatrix} \boldsymbol{L}_{1,1} & ... & \boldsymbol{L}_{1,N_{all}} \\ \vdots & \ddots & \vdots \\ \boldsymbol{L}_{N_{dc},1} & ... & \boldsymbol{L}_{N_{dc},N_{all}} \end{bmatrix}. \tag{30}$$

The i^{th} row, j^{th}column block of $\boldsymbol{L}$ is:

$$\boldsymbol{L}_{i,j} = (\boldsymbol{P}^T)_{i,j}\boldsymbol{I}_{N_{bs}}. \tag{31}$$

$\boldsymbol{C}$ is a block matrix:

$$\boldsymbol{C} = \begin{bmatrix} \boldsymbol{C}_{1,1} & \boldsymbol{C}_{1,2} \\ \vdots & \vdots \\ \boldsymbol{C}_{N_{dc},1} & \boldsymbol{C}_{N_{dc},2} \end{bmatrix}. \tag{32}$$

The i^{th} row, j^{th} column block of $\boldsymbol{C}$ is:

$$\boldsymbol{C}_{i,j} = (\boldsymbol{P}^T\boldsymbol{F}_P)_{i,j}\boldsymbol{I}_{N_{bs}}, \tag{33}$$

where $i = 1, 2, ..., N_{dc}$ and $j = 1, 2$.

The total energy absorbed by the WEC is:

$$\begin{aligned} J &= -\int_0^T [\boldsymbol{P}\boldsymbol{\Psi}\hat{\boldsymbol{V}}_s]^T\boldsymbol{F}_P\boldsymbol{\Psi}_{2\times N_{bs}}\hat{\boldsymbol{U}}_c dt \\ &= -\frac{T}{2}\hat{\boldsymbol{V}}_s^T\boldsymbol{C}\hat{\boldsymbol{U}}_c, \end{aligned} \tag{34}$$

and the mean power is defined as:

$$\overline{J} = \frac{1}{2}\hat{\boldsymbol{V}}_s^T\boldsymbol{C}\hat{\boldsymbol{U}}_c. \tag{35}$$

The control parameter optimization issue is mathematically defined as:

$$\begin{aligned} &Minimize\ \ \overline{J} = \frac{1}{2}\hat{\boldsymbol{V}}_s^T\boldsymbol{C}\hat{\boldsymbol{U}}_c \\ &Subject\ to: \boldsymbol{H}\hat{\boldsymbol{V}}_s = \boldsymbol{L}\hat{\boldsymbol{E}} + \boldsymbol{C}\hat{\boldsymbol{U}}_c. \end{aligned} \tag{36}$$

V. Geometric Optimization

The overall optimization objective is to find the optimal geometric design parameters, with the optimized PTO control parameters, for the given sea state. This is an energy-maximization optimization problem [24], with two geometric design variables to be optimized, i.e. the length of fore barge $L1$ and the length of the aft barge $L3$. Figure 2 illustrates the optimization procedure, and it shows that the optimization of geometric design variables and the optimization of PTO control parameters are integrated in the overall optimization.

For each defined WEC geometry set, a discretized mesh is created to approximately describe the wet surface of rigid bodies and used in the hydrodynamic model. Hydrodynamic parameters, e.g., added mass, are computed based on linear potential flow theory, assuming the motion of the floating device is small so that the boundary conditions are satisfied. Multiple methods can be employed to approach the solution, e.g., the genetic algorithm and exhaustive search method.

Within the overall optimization routine, PTO damping coefficients are optimized for each considered geometry set, and the given sea state, by solving the formulated optimization problem described in previous section. The optimized fore and aft PTO damping coefficients yield maximum energy for the considered geometry in the given sea state. Figure 3 shows the detailed variation of capture width ratio for a device with $L1 = 0.4m$ and $L3 = 0.4m$, over different damping coefficients for fore and aft PTOs. These optimal linear PTO damping coefficients are used in the computation of mean power.

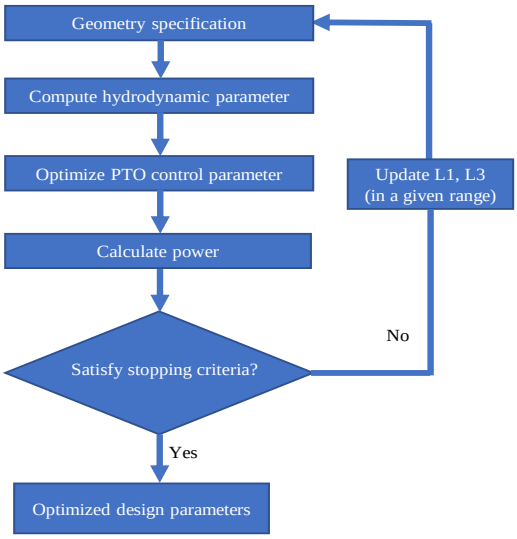

Fig. 2. Scheme of control-informed geometry optimization.

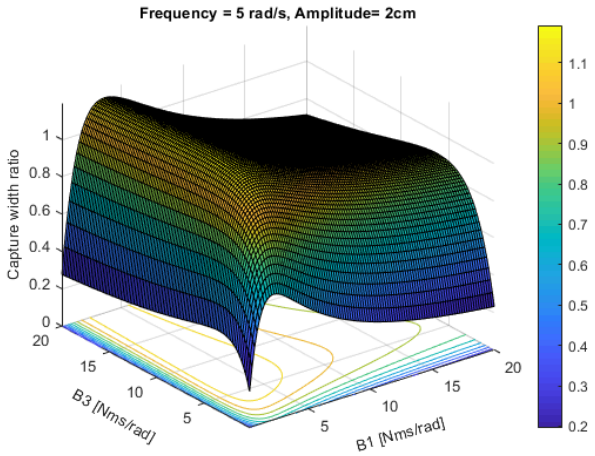

Fig. 3. Variation of capture width ratio over PTO damping coefficients for the geometry set with L1 = 0.4 m, L2 = 0.28 m and L3 = 0.4 m. Passive controllers are employed by PTOs.

An energy-maximization based index is employed to evaluate the performance of each geometry set during the overall optimization routine, and the geometry set with maximum energy generation is selected as the optimal geometric design parameters.

VI. RESULTS

Simulations are carried out in MATLAB, with the algorithm used for solving the PTO optimization problem is implemented by the $fmincon$ function included in the MATLAB Optimization Toolbox and the approach used for selecting the optimal geometric design parameters is achieved by employing the exhaustive search method. Hydrodynamic parameters, including added mass, radiation damping coefficients and excitation force coefficients are computed in WAMIT [25], a boundary element method code based on the linear potential flow theory. The flow is assumed as ideal, i.e., inviscid and irrorational in the fluid domain, thereby the flow velocity potential satisfies the Laplace equation and boundary conditions.

E. Simulation parameters

The overall dimensions of the original $1/25^{th}$ McPump prototype are $2.01\ m \times 0.4\ m \times 0.15\ m$ (i.e., length $\times$ width $\times$ height). The original dimensions of the fore barge are $0.68m \times 0.4m \times 0.1m$, $0.28m \times 0.4m \times 0.15\ m$ for the central barge, and the original dimensions of the aft barge are $1.0m \times 0.4m \times 0.1m$. A damping plate with dimensions $0.4m \times 0.4m \times 0.03m$ is affixed to the central barge to limit heave, and it is lowered 0.127 m below the bottom of the central barge. The spacing between any two neighboring barges in still water is 0.06 m. In the following context, fore barge length $L1$ and aft barge length $L3$ are the design parameters to be optimized, while the geometric parameters of the central barge are kept as for the original prototype.

We assume both of the two PTOs are equipped with an optimal linear passive controller, and the PTO damping coefficients vary from 0 to 50 Nms/rad, depending on the sea state and geometry parameters. Table II shows ranges of design and control parameters used in simulation. The lengths of fore barge and of aft barge vary from 0.1 m to 2.0 m with a step of 0.1 m.

TABLE II
RANGES OF CONTROL AND GEOMETRY DESIGN PARAMETERS

Range	**Parameters**			
	B1 [Nms/rad]	B2 [Nms/rad]	L1 [m]	L3 [m]
Min.	0	0	0.1	0.1
Max.	50	50	2.0	2.0

F. Results under regular waves

1) Initial regular wave test: Consider a regular wave with an amplitude of 0.02 m and an angular frequency of 4 rad/s, the proposed methodology is employed to optimize the geometric design parameters $L1$ and $L3$.

As indicated in Table III, the optimal length of the fore barge is close to the value of the original $1/25^{th}$ prototype, while the optimal length of the aft barge is 50% larger than the original prototype. The mean power of the optimized device under this sea state is 1.1 W, while the mean power of the original $1/25^{th}$ prototype is 0.9 W. This indicates that the electricity generation can be improved by 22% in this sea state by the geometric optimization method.

TABLE III
OPTIMIZED GEOMETRY DESIGN PARAMETERS UNDER A REGULAR WAVE WITH AN AMPLITUDE OF 0.02 M AND A FREQUENCY OF 4 RAD/S

Barge Name	**Optimal Length**
Fore barge	0.7 m
Aft barge	1.5 m

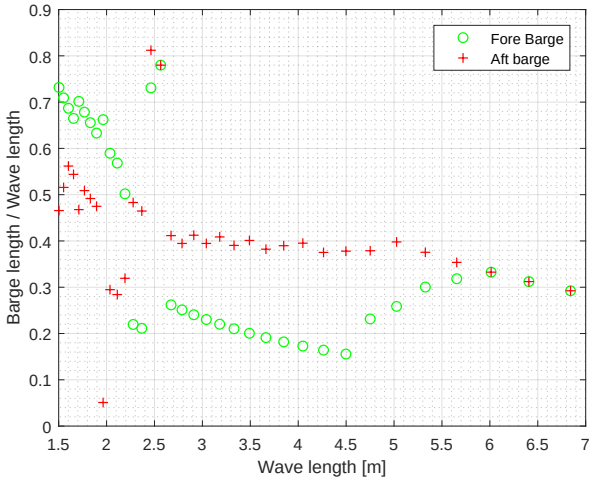

Fig. 4. Optimized lengths of fore barge and aft barge in different wave lengths. The length of central barge is fixed as $0.28m$. The PTOs are equipped with optimal linear passive controllers. The wave amplitude is fixed as 2 cm.

2) Further regular wave tests: The hinge-barge WEC has a broad frequency response with respect to incident waves. It is meaningful to investigate the optimal geometric lengths of the device in different incident wave conditions. The optimized results given by the proposed control-informed geometric optimization are shown in Figure 4.

It is found that, in general, the optimal length of fore barge is greater than that of the aft barge in short wavelengths and is much less than the aft barge in long wavelengths. The optimal length of the aft barge is about 0.4 times the length of the incident wave and the optimal length of the aft barge varies in a range of 0.15-0.35 times the length of incident wave, in long wavelengths.

G. Results under irregular waves

Polychromatic waves can be created as a linear combination of monochromatic waves using a ocean-wave spectrum, defined by a significant wave height, a peak period, and random phases [26]. In this section, the polychromatic wave is created using the Pierson-Moskowitz spectrum, with a significant wave height of $H_s = 4.82\,cm$ and a peak period of $T_p = 1.1\,s$, which is scaled down from one of the most common sea states in Galway Bay, off the west coast of Ireland. The resulting wave load acting on the WEC is computed using WAMIT.

Table IV summarizes the optimization results for the considered irregular waves. It shows that the optimal length of the aft barge is greater than that of the fore barge. Figure 5 presents the instantaneous power of the optimized WEC equipped with optimal linear PTO passive controllers, under this irregular wave. It is found that the fore PTO generates more energy, compared to the aft PTO, with the fore PTO having a mean power of 0.18 W, while the aft PTO has a power of 0.08 W, which means the fore PTO contributes 70% of the total energy production. In addition, compared with the original prototype, the geometric optimization improves the energy production from 0.14 W to 0.26 W. The increment ratio is 78.6% for the given irregular waves.

TABLE IV
OPTIMIZED GEOMETRIC DESIGN PARAMETERS UNDER THE IRREGULAR WAVES WITH $H_s = 4.82\,cm$ AND $T_p = 1.1\,s$

Barge Name	Optimal Length
Fore barge	0.1 m
Aft barge	1.3 m

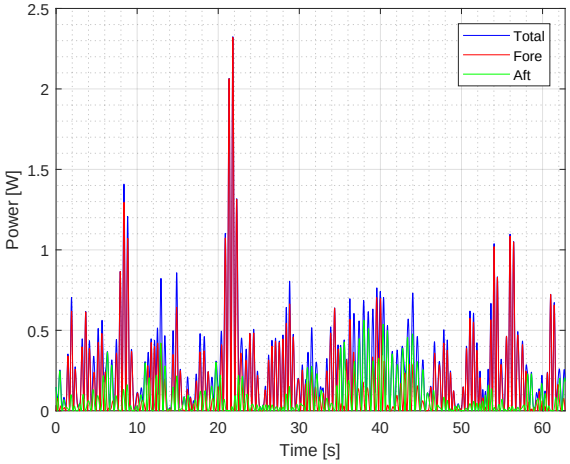

Fig. 5. Instantaneous power of the device with optimized geometric parameters and optimized PTO control parameters, for irregular waves with $H_s = 4.82\,cm$ and $T_p = 1.1\,s$.

VII. DISCUSSION

hH. Geometric optimization for long-term operation

The previous section presents the optimal geometric parameters of a three-body hinge-barge WEC under multiple regular waves and an irregular wave. Results indicate that energy production of the WEC can be improved in these independent incident waves. However, WECs are expected to work in a sea site for a long term, which means only one geometry set will be used in the construction of the full-scale prototype and is normally fixed after deployment. In addition, the deployed WEC will encounter different incident waves during long-term operation. As illustrated in Figure 6, the statistical analysis of the measured ocean waves at Galway Bay in January 2017 shows that the values and occurring frequency of significant wave height and peak energy period vary over a wide range. It is therefore meaningful to determine the optimal geometric design parameters with a long-term perspective.

To approach that, a new evaluation/selection function is proposed to evaluate the total energy production of the WEC in the long term, considering all likely sea states. Sea state information can be gleaned from historical measurements and/or prediction of future

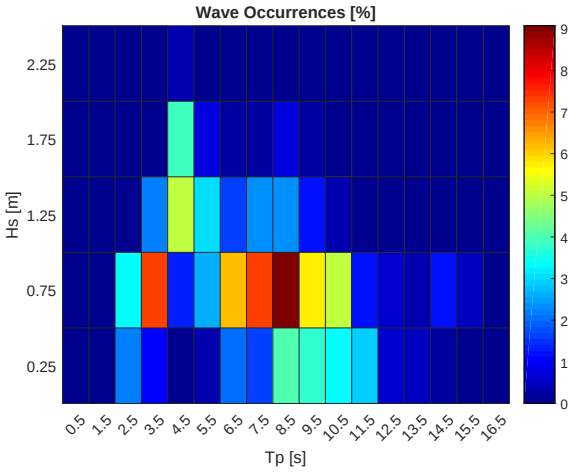

Fig. 6. Scatter diagram of the measured ocean waves in Galway Bay, off west coast of Ireland, in January 2017. Raw data can be found at [27].

ocean waves. The evaluation function to select the optimal geometric design parameters over a long term is defined as:

$$E_{acc}(L1, L3) = \sum_{j=1}^{N_s} f(j)P(j, L1, L3), \tag{37}$$

where j is an index of the sea state that is from measurement or prediction in the short term, e.g, half an hour, N_s is the total number of sea states considered, $f(j)$ is a weight function, referring to the likelihood of occurrance of sea state j in the long term, $P(j, L1, L3)$ represents the generated mean power of one geometry set of $L1$ and $L3$ in sea state j. Thereby, E_{acc} is an index proportional to the total energy generation of a particular geometry set in the long term.

Table V presents the long-term optimization results for the hinge-barge prototype. The sea state values are scaled down from the historical data presented in Figure 6, based on the principle of Froude scaling. Results indicate that both the optimal fore barge length and the optimal aft barge length should be greater than the original design values, for this deployment site.

TABLE V
OPTIMIZED DESIGN GEOMETRY PARAMETER IN LONG TERM

Barge Name	Optimal Length
Fore barge	1.4 m
Aft barge	1.8 m

I. *Two barges or three barges?*

Results in Figure 3 also show that the WEC with this geometry set ($L1 = 0.4m, L2 = 0.28m, L3 = 0.4m$) has a trend to perform like a two-body system, as the the total energy production tends to approach an upper bound constant when increasing the aft PTO damping to high values, where the central barge and the aft barge will perform like one rigidly connected body.

Extending the investigation to more geometry settings reveals that the two-body-like trends are maintained. A relative low, yet optimal, damping value is suggested for the fore PTO to maximize the total energy generation while high damping values are suggested for the other PTO that yields a two-body performance. As presented in Figure 7(a), the optimal damping coefficient of the fore PTO, i.e. $B1^*$, increases with barge length. As presented in Figure 7(b), the ratio of suggested optimal PTO damping coefficients for each geometry set is held at a high value.

The fact that the three-body hinge-barge WEC acts like a two-body system in the optimal control condition (passive control in this study) is meaningful to both the designers of a physical device and of for PTO control. It is well-known that, among all material costs, capital cost of PTOs and controllers are high. Therefore, if the optimal geometric parameters and PTO configurations are properly ascertained, the techno-economic performance [28] [29] of hinge-barge WECs can be significantly improved.

VIII. CONCLUSIONS

In this work, a methodology for control-informed geometric optimization of a hinge-barge wave energy converter (WEC) is presented, based on an embedding technique for modeling multi-body systems and a spectral method for solving the equation of motion. The optimization process is applied to a three-body hinge-barge WEC that is originally from a $1/25^{th}$ protytope hinge barge. This WEC has 5 degrees of freedom and is equipped with two optimal linear passive PTO controllers.

The simultaneous design of device geometry and PTO control parameters yields better performance, in terms of energy generation. However, the optimal geometry depends on incident waves, on a short-term perspective, e.g., the optimal length of the fore barge varies in a range of 0.15-0.35 times the length of incident waves and the optimal length of aft barge is about 0.4 times the length of incident waves. As indicated in the pilot study, the three-body hinge-barge WEC with a fore barge length of $1.4\,m$ and an aft barge length of $1.8\,m$ has a higher energy generation, with the long-term perspective.

It can be concluded that the three-body hinge-barge WEC acts like a two-body control system in the optimal control condition (optimal linear passive control is employed in this study). From a techno-economic perspective, it is meaningful to perform further analysis on the benefits of employing two PTO control systems or one PTO control system, by considering the capital cost of PTO control systems and considering electricity generation of PTOs over the long term.

It should be noted that this method is based on a linearised model and the linear potential flow theory, which limits its application to linear waves and small amplitude motions. It is of further interest to investigate the implications of such limitations.

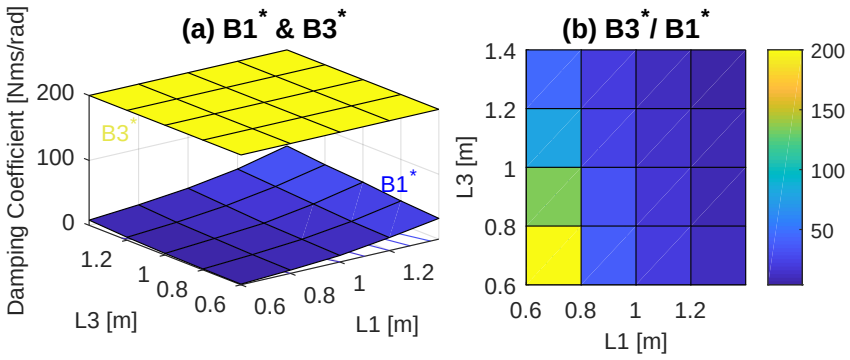

Fig. 7. Values and ratio of fore PTO coefficient $B1^*$ and aft PTO coefficient $B3^*$ that maximize the energy generation and yield a two-barge performance. (a) Detailed values. (b) Ratio.

APPENDIX A
INNER PRODUCT

Formally:

$$\int_0^{T_0} \boldsymbol{\Phi}(t)\boldsymbol{\Phi}^T(t)dt = \frac{T}{2}\boldsymbol{I}_{N_{bs}}, \tag{38}$$

$$\langle \phi_i, \phi_j \rangle = \int_0^T \phi_i(t)\phi_j(t)dt = \frac{T}{2}\delta_{ij}, \tag{39}$$

where $\boldsymbol{I}_{N_{bs}}$ is an identity matrix of size N_{bs}, and δ_{ij} is the Kronecker delta.

In a concise form,

$$\begin{aligned}&\langle \boldsymbol{\Phi}, \sum_{p=1}^{N_{dc}} (\boldsymbol{M}_s + \boldsymbol{M}_{\infty s})_{i,p}\boldsymbol{\Phi}^T(t)\boldsymbol{D}\rangle \hat{\boldsymbol{v}}_p \\ &= \frac{T}{2}\sum_{p=1}^{N_{dc}} (\boldsymbol{M}_s + \boldsymbol{M}_{\infty s})_{i,p}\boldsymbol{D}\hat{\boldsymbol{v}}_p,\end{aligned} \tag{40}$$

$$\begin{aligned}&\langle \boldsymbol{\Phi}, \sum_{p=1}^{N_{dc}} (\boldsymbol{B}_s + \boldsymbol{B}_{visc,s})_{i,p}\boldsymbol{\Phi}^T(t)\hat{\boldsymbol{v}}_p\rangle \\ &= \frac{T}{2}\sum_{p=1}^{N_{dc}} (\boldsymbol{B}_s + \boldsymbol{B}_{visc,s})_{i,p}\boldsymbol{I}_{N_{bs}}\hat{\boldsymbol{v}}_p,\end{aligned} \tag{41}$$

$$\begin{aligned}\langle \boldsymbol{\Phi}, \sum_{p=1}^{N_{dc}} (\boldsymbol{G}_s)_{i,p}\boldsymbol{\Phi}^T\hat{\boldsymbol{x}}_p\rangle &= \frac{T}{2}\sum_{p=1}^{N_{dc}} (\boldsymbol{G}_s)_{i,p}\boldsymbol{I}_{N_{bs}}\hat{\boldsymbol{x}}_p \\ &= \frac{T}{2}\sum_{p=1}^{N_{dc}} (\boldsymbol{G}_s)i,p\boldsymbol{D}^{-1}\hat{\boldsymbol{v}}_p,\end{aligned} \tag{42}$$

$$\langle \boldsymbol{\Phi}, (\boldsymbol{P}^T\boldsymbol{\Psi}_e(t)\hat{\boldsymbol{E}})_i\rangle = \frac{T}{2}\sum_{j=1}^{N_{all}} (\boldsymbol{P}^T)_{i,j}\boldsymbol{I}_{N_{bs}}\hat{\boldsymbol{e}}_i, \tag{43}$$

$$\begin{aligned}&\langle \boldsymbol{\Phi}, (\boldsymbol{P}^T\boldsymbol{F}_P\boldsymbol{\Psi}_{2*2N_{bs}}\hat{\boldsymbol{U}}_c)_i\rangle = \int_0^T \boldsymbol{\Phi}(t)(\boldsymbol{P}^T\boldsymbol{F}_P)_{i,j}\boldsymbol{u}_j(t)dt \\ &= \int_0^T \sum_{i=1}^{2} \boldsymbol{\Phi}(t)(\boldsymbol{P}^T\boldsymbol{F}_P)_{i,j}\boldsymbol{u}_j(t)dt = \sum_{j=1}^{2}\frac{T}{2}(\boldsymbol{P}^T\boldsymbol{F}_p)_{i,j}\hat{\boldsymbol{u}}_j.\end{aligned} \tag{44}$$

The radiation force is

$$\langle \boldsymbol{\Phi}, \sum_{p=1}^{N_{dc}} \int_0^t K_{i,p}(t-\tau)\boldsymbol{\Phi}^T(\tau)\hat{\boldsymbol{v}}_p d\tau\rangle = \frac{T}{2}\sum_{p=1}^{N_{dc}} \boldsymbol{G}_{i,p}\hat{\boldsymbol{v}}_p. \tag{45}$$

$\boldsymbol{G}_{i,p}$ is a block diagonal matrix with $N_{bs}/2$ blocks:

$$\boldsymbol{G}_{i,p} = \begin{bmatrix} \boldsymbol{G}_{i,p}^1 & & \\ & \boldsymbol{G}_{i,p}^2 & \\ & \ddots & \\ & \dots & \boldsymbol{G}_{i,p}^{N_{bs}/2} \end{bmatrix}, \tag{46}$$

and its k_{th} block is:

$$\boldsymbol{G}_{i,p}^k = \begin{bmatrix} R_{i,p}(kw_0) & kw_0(B_{i,p}(kw_0) - M_{\infty i,p}) \\ -kw_0(B_{i,p}(kw_0) - M_{\infty i,p}) & R_{i,p}(kw_0) \end{bmatrix}, \tag{47}$$

where $R_{i,k}(kw_0)$ is the added mass, and $B_{i,p}(kw_0)$ is the radiation damping coefficient. They are frequency dependent values.

ACKNOWLEDGEMENT

This paper is based on upon work supported by Science Foundation Ireland under Grant No. SFI/13/IA/1886 and Grant No. 12/RC/2302 for MaREI Centre for Marine and Renewable Energy.

REFERENCES

[1] J. Goggins and W. Finnegan, "Shape optimisation of floating wave energy converters for a specified wave energy spectrum," *Renewable Energy*, vol. 71, pp. 208–220, Nov. 2014.

[2] M. Shadman, S. F. Estefen, C. A. Rodriguez, and I. C. M. Nogueira, "A geometrical optimization method applied to a heaving point absorber wave energy converter," *Renewable Energy*, vol. 115, pp. 533–546, Jan. 2018.

[3] H. Shi, Z. Han, and C. Zhao, "Numerical study on the optimization design of the conical bottom heaving buoy convertor," *Ocean Engineering*, vol. 173, pp. 235–243, Feb. 2019.

[4] A. Babarit, A. H. Clément, and J.-C. Gilloteaux, "Optimization and time-domain simulation of the searev wave energy converter," in *ASME 2005 24th International Conference on Offshore Mechanics and Arctic Engineering*. American Society of Mechanical Engineers, 2005, pp. 703–712.

[5] A. Kurniawan and T. Moan, "Multi-objective optimization of a wave energy absorber geometry," *Proceedings of the 27th International Workshop on Water Waves and Floating Bodies, Copenhagen, Denmark*, pp. 1–4, 2012.

[6] A. P. McCabe, "Constrained optimization of the shape of a wave energy collector by genetic algorithm," *Renewable Energy*, vol. 51, pp. 274–284, Mar. 2013.

[7] J.-C. Gilloteaux and J. Ringwood, "Control-informed geometric optimisation of wave energy converters," *IFAC Proceedings Volumes*, vol. 43, no. 20, pp. 366–371, Sep. 2010.

[8] P. B. Garcia-Rosa, G. Bacelli, and J. V. Ringwood, "Control-informed geometric optimization of wave energy converters: The impact of device motion and force constraints," *Energies*, vol. 8, no. 12, pp. 13 672–13 687, 2015.

[9] P. B. Garcia-Rosa and J. V. Ringwood, "On the sensitivity of optimal wave energy device geometry to the energy maximizing control system," *IEEE Transactions on Sustainable Energy*, vol. 7, no. 1, pp. 419–426, Jan 2016.

[10] P. B. Garcia-Rosa, G. Bacelli, and J. V. Ringwood, "Control-informed optimal array layout for wave farms," *IEEE Transactions on Sustainable Energy*, vol. 6, no. 2, pp. 575–582, April 2015.

[11] L. Sun, J. Zang, P. Stansby, E. C. Moreno, P. H. Taylor, and R. E. Taylor, "Linear diffraction analysis of the three-float multi-mode wave energy converter m4 for power capture and structural analysis in irregular waves with experimental validation," *Journal of Ocean Engineering and Marine Energy*, vol. 3, no. 1, pp. 51–68, Feb 2017.

[12] F. Paparella and J. V. Ringwood, "Optimal control of a three-body hinge-barge wave energy device using pseudospectral methods," *IEEE Transactions on Sustainable Energy*, vol. 8, no. 1, pp. 200–207, Jan 2017.

[13] X. Zhang, D. Lu, F. Guo, Y. Gao, and Y. Sun, "The maximum wave energy conversion by two interconnected floaters: Effects of structural flexibility," *Applied Ocean Research*, vol. 71, pp. 34 – 47, 2018.

[14] S. Zheng and Y. Zhang, "Analysis for wave power capture capacity of two interconnected floats in regular waves," *Journal of Fluids and Structures*, vol. 75, pp. 158–173, Nov. 2017.

[15] M. McCormick, J. Murthagh, and P. McCabe, "Large-scale experimental study of a hinged-barge wave energy conversion system," *Proceedings of the 3rd European Wave Energy Conference, Patras, Greece*, pp. 215–222, 1998.

[16] D. Padeletti, R. Costello, and J. V. Ringwood, "A multi-body algorithm for wave energy converters employing nonlinear joint representation," in *ASME 2014 33rd International Conference on Ocean, Offshore and Arctic Engineering*. American Society of Mechanical Engineers, Jun. 2014, p. V09AT09A052.

[17] L. Sun, R. E. Taylor, and Y. S. Choo, "Responses of interconnected floating bodies," *The IES Journal Part A: Civil & Structural Engineering*, vol. 4, no. 3, pp. 143–156, Aug. 2011.

[18] H.-F. Yu, Y.-L. Zhang, and S.-M. Zheng, "Numerical study on the performance of a wave energy converter with three hinged bodies," *Renewable Energy*, vol. 99, pp. 1276 – 1286, 2016.

[19] F. Paparella, G. Bacelli, A. Paulmeno, S. E. Mouring, and J. V. Ringwood, "Multibody modelling of wave energy converters using pseudo-spectral methods with application to a three-body hinge-barge device," *IEEE Transactions on Sustainable Energy*, vol. 7, no. 3, pp. 966–974, July 2016.

[20] A. A. Shabana, *Dynamics of Multibody Systems*, 4th ed. Cambridge University Press, 2013.

[21] G. Bacelli, "Optimal control of wave energy converters," Ph.D. dissertation, National University of Ireland Maynooth, Maynooth, Ireland, 2014.

[22] F. Paparella, "Modeling and control of a multibody hinge-bargewave energy converter," Ph.D. dissertation, National University of Ireland Maynooth, Maynooth, Ireland, 2017.

[23] F. Paparella and J. V. Ringwood, "Optimal control of a three-body hinge-barge wave energy device using pseudospectral methods," *IEEE Transactions on Sustainable Energy*, vol. 8, no. 1, pp. 200–207, Jan 2017.

[24] J. V. Ringwood, G. Bacelli, and F. Fusco, "Energy-maximizing control of wave-energy converters: The development of control system technology to optimize their operation," *IEEE Control Systems Magazine*, vol. 34, no. 5, pp. 30–55, Oct 2014.

[25] [Online]. Available: http://www.wamit.com

[26] U. A. Korde and J. Ringwood, *Hydrodynamic Control of Wave Energy Devices*. Cambridge University Press, 2016.

[27] [Online]. Available: http://www.oceanenergyireland.com/Observation/DownloadWave

[28] R. Costello, B. Teillant, J. Weber, and J. Ringwood, "Techno-economic optimisation for wave energy converters," in *4th International Conference on Ocean Energy*, Dublin, Ireland, 2012, pp. 1–5.

[29] A. de Andres, J. Maillet, J. Hals Todalshaug, P. Mller, D. Bould, and H. Jeffrey, "Techno-economic related metrics for a wave energy converters feasibility assessment," *Sustainability*, vol. 8, no. 11, p. 1109, 2016.